International Journal of Advanced Engineering Research and Science (IJAERS)
Peer-Reviewed Journal
ISSN: 2349-6495(P) | 2456-1908(O)
Vol-13, Issue-3; Mar, 2026
Journal Home Page Available: https://ijaers.com/
Article DOI: https://dx.doi.org/10.22161/ijaers.133.3

Improving NSGA-II using a Dynamic Average Distance Selection Strategy

Jie-Zhen Yang, Yan-Zuo Chang*, Qi-Hong Tang, Guan-Hong Xie, Yong-Qing Wang, Zheng-Kuan Deng, Zi-Rui He, Kai-Ming Chen, Yu-Xuan Chen, Hong-Rui Yang, Wen-Min Wen

School of Energy and Power Engineering, Guangdong University of Petrochemical Technology, Maoming, Guangdong 525000, China
*Corresponding Author

Received: 21 Jan 2026,

Received in revised form: 17 Feb 2026,

Accepted: 22 Mar 2026,

Available online: 26 Mar 2026

***Keywords*— NSGA-II, multi-objective optimization, dynamic average distance, Spacing indicator, ZDT series test functions.**

***Abstract*—** *The traditional Non-dominated Sorting Genetic Algorithm II (NSGA-II) struggles to maintain a uniformly distributed solution set across the entire Pareto front when dealing with non-uniform, non-convex, or discontinuous Pareto fronts. This limitation arises because its crowding distance metric relies solely on local linear spacing, making it prone to issues such as the loss of boundary solutions or local redundant clustering. To address this problem, this paper proposes an improved NSGA-II algorithm, whose core mechanism is the introduction of a dynamic average distance selection strategy into the original framework. Instead of using the traditional local crowding distance metric, the proposed algorithm constructs an "influence rectangle" for each individual using a dynamic scaling factor. This transforms the occupancy relationship of individuals in the objective space into the degree of geometric overlap between these rectangles, enabling the identification and elimination of redundant individuals. Experiments are conducted using ZDT series test functions, and the Spacing (SP) indicator is employed to evaluate the distribution uniformity of the obtained solution sets. Simulation results demonstrate that, while maintaining good convergence, the SP indicator values of the improved algorithm on the ZDT1, ZDT2, and ZDT3 test functions are significantly reduced, with a decrease ranging from 56.10% to 59.10%. This fully verifies the effectiveness of the dynamic average distance strategy in enhancing the distribution uniformity of the solution set. When addressing problems with discontinuous and concave fronts, the algorithm exhibits excellent robustness and uniform distribution capability. By incorporating an adaptive geometric evaluation criterion, the improved NSGA-II algorithm provides more reliable and stable decision support for complex multi-objective optimization problems.*

I. INTRODUCTION

Multi-objective optimization problems (MOPs) are prevalent in numerous important fields such as energy scheduling, computing resource allocation, engineering design, and machine learning. The objective in solving such problems is to find a set of Pareto optimal solutions that strike a balance between convergence and distribution among multiple conflicting objectives. Evolutionary multi-

objective optimization algorithms, with their powerful parallel search capability within a population, have become one of the mainstream methods for solving such problems. Among these, NSGA-II is recognized as the most representative benchmark algorithm due to its two core mechanisms: fast non-dominated sorting and crowding distance. However, as the complexity of real-world problems continues to increase, maintaining a uniform distribution of the solution set in large-scale, high-dimensional, or even discontinuous objective spaces remains a critical breakthrough point in the design of algorithmic improvements.

To address the shortcomings in the diversity maintenance mechanism of NSGA-II, numerous studies have been conducted by researchers worldwide to improve the algorithm. [1][2][3] Most of this work focuses on modifying the crowding distance, introducing strategies such as angle information, density estimation, and adaptive neighborhoods to mitigate local clustering. Other studies draw on ideas from clustering, grid partitioning, or reference point guidance to reconstruct the environmental selection criteria, aiming to enhance the spread of the solution set. For instance, the reference-point-based NSGA-III performs well in handling many-objective problems, but its distribution performance is highly dependent on the pre-defined locations of the reference points. Although the methods mentioned above improve the distribution uniformity of the algorithm to varying degrees, they still struggle to avoid issues like the loss of boundary solutions or redundant clustering within segmented intervals when faced with non-uniform, non-convex, or discontinuous Pareto fronts. The fundamental reason lies in the fact that most traditional methods measure diversity based on local linear distances or fixed structures, and these approaches generally lack a holistic understanding of the global occupancy relationship of the population within the objective space .[4][5][6]

Addressing the limitations of the traditional NSGA-II algorithm discussed above, this paper proposes an improved NSGA-II algorithm based on a dynamic average distance selection strategy. This algorithm incorporates a dynamic scaling factor to assist in constructing an influence rectangle model for each individual. This transformation shifts the diversity measure from a one-dimensional linear distance to a multi-dimensional assessment of geometric overlap. By quantifying the degree of overlap between these rectangles, the method can accurately identify and iteratively eliminate redundant individuals, allowing for the flexible adaptation and adjustment of the screening granularity during the evolutionary process. Comparative experiments on ZDT series test functions verify that the dynamic average distance selection strategy effectively enhances distribution uniformity and exhibits good robustness on discontinuous and concave fronts.

II. IMPROVEMENT STRATEGY FOR THE NSGA-II ALGORITHM

2.1 Traditional NSGA-II Algorithm

The core mechanisms of the traditional NSGA-II algorithm include fast non-dominated sorting and crowding distance.[7][8] The crowding distance maintains population distribution by measuring the local spacing between an individual and its neighbors. Its calculation is straightforward, leading to its widespread application in the field of multi-objective optimization. However, this metric only reflects one-dimensional linear spacing and fails to capture the global occupancy relationships of the solution set within the objective space. When dealing with non-uniform or discontinuous fronts, individuals in dense regions may be misjudged as sparse, and critically important boundary solutions are prone to loss during the selection process. This limitation restricts the distribution performance of NSGA-II on complex front topologies.

2.2 Core Mechanisms of the Improved NSGA-II Algorithm

The key mechanisms of the improved algorithm primarily revolve around three aspects: the dynamic average distance, the influence rectangle, and the degree of overlap. The dynamic average distance serves as a benchmark for global distribution. Its calculation is based on the range of the current non-dominated layer across all objectives and the population size. It transforms each individual into an "influence rectangle" with a specific scale, thereby converting the spatial distribution of solutions into a geometric occupancy problem. The improved algorithm further identifies locally dense regions by quantifying the degree of overlap between the influence rectangles of neighboring individuals. These three mechanisms collectively lay the foundation for the subsequent elimination of redundant individuals.

2.2.1 Dynamic Average Distance and Its Scaling

In the traditional algorithm, the crowding distance fails to reflect the overall distribution state of the population in the objective space, as it can only derive the local spacing between neighboring individuals. To maintain a similar density of solution distribution across different regions, a global reference scale that can be flexibly adjusted during the evolutionary process is required. The dynamic average distance is calculated based on the range of the current non-dominated layer on each objective and the population size, and its value is updated as the population distribution

evolves. Using this as a foundation for unit scaling, the influence rectangle for each individual is constructed through the dynamic scaling factor *Mu*, allowing the sensitivity of the subsequent geometric overlap assessment to be adjusted according to the actual density.

To establish a global distribution reference, the dynamic average distance *Mu* is introduced. The dynamic average distance on the m-th objective, $D(f_m)$ is defined. Its calculation is based on the objective range of individuals in the current non-dominated layer:

$$D(f_m) = \frac{f_m^{\max} - f_m^{\min}}{N} \tag{1}$$

Here, $f_m^{\max}$ and $f_m^{\min}$ are the maximum and minimum boundary values of the current population on the m-th objective, respectively, and *N* is the population size. The dynamic scaling factor *Mu* is introduced to construct an influence range centered on each individual.

Let the dynamic average distance on the m-th objective be D_m, whose definition is given by equation (1). The boundaries of the influence rectangle for individual ii on objective m are defined as:

$$L_{i,m} = f_m(\mathbf{x}_i) - \frac{Mu \cdot D_m}{2}, R_{i,m} = f_m(\mathbf{x}_i) + \frac{Mu \cdot D_m}{2} \tag{2}$$

Here, $f_m(\mathbf{x}_i)$ is the function value of individual i on the m-th objective.

2.2.2 Influence Rectangle and Overlap Degree Model

The influence range of an individual in the objective space is jointly determined by the dynamic average distance D_m and the scaling factor *Mu*. Each individual *i*, centered at its objective function value $f_m(\mathbf{x}_i)$, extends outward by a distance of $Mu \cdot D_m / 2$ on each side, forming the influence interval of this individual on the m-th objective. Combining the influence intervals across all objectives yields the two-dimensional influence rectangle of the individual in the objective space. Figure 1 illustrates this process of constructing an individual's influence rectangle in the objective space using the dynamic average distance, along with its geometric significance.

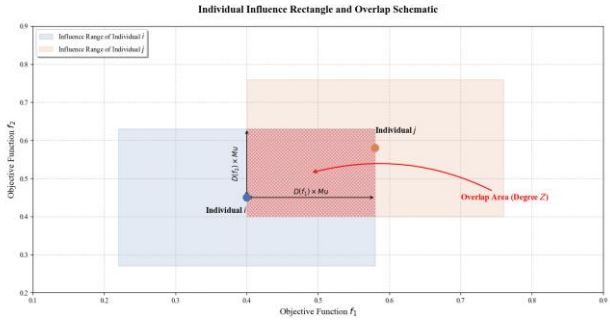

Fig. 1: Schematic diagram of individual influence rectangles and overlap degree

The overlap degree $Z_{m,i}$ between neighboring individuals on the m-th objective is defined as:

$$Z_{m,i} = \frac{2D(f_m) - |d_{m,i-1}^b - d_{m,i}^s|}{D(f_m)} \tag{3}$$

Here, $d_{m,i-1}^b$ represents the right and upper boundaries of the influence rectangle of the preceding individual, and $d_{m,i}^s$ represents the left and lower boundaries of the influence rectangle of the current individual. The overlap degree *Z* is used to reflect the density of individual distribution.

Figure 1 illustrates the geometric representation logic of the individual influence rectangle and the overlap measure. This figure represents individuals in the objective space as influence regions with specific dimensions, thereby establishing a distribution evaluation model based on spatial occupancy. By transforming the abstract density of the solution set into a visualizable overlap distance, this model provides a more concrete and intuitive physical criterion for identifying and quantifying local clustering phenomena on the Pareto front. This also serves as an important logical foundation for the subsequent elimination of redundant individuals. On a mathematical level, the above model ensures the rigor of the dynamic average distance selection strategy in maintaining the distribution uniformity of the population.

III. ALGORITHM FLOW

The improved algorithm retains the fast non-dominated sorting and genetic operators (crossover, mutation) of NSGA-II, with the core improvement lying in the environmental selection stage. In this stage, the dynamic average distance strategy is introduced to finely regulate the distribution of the population.

3.1 Overall Algorithm Framework

The main framework of the improved algorithm still follows the basic paradigm of evolutionary multi-objective optimization. First, a population of size N is randomly initialized, and offspring are generated through crossover and mutation. Subsequently, the parent and offspring populations are merged to form a combined population of size $2N$. Through fast non-dominated sorting, the population is divided into different Pareto layers (F_1 , F_2 ,…) . While populating the next generation, individuals from each layer are added sequentially until the inclusion of a certain layer (the critical layer F_k) causes the population size to exceed the limit N. At this point, instead of using the traditional crowding distance calculation, the algorithm employs the dynamic redundancy elimination mechanism proposed in this paper.

3.2 Environmental Selection Logic based on Geometric Overlap

During the selection process for the critical layer F_k , the improved NSGA-II algorithm performs calculations based on equation (1) to determine the dynamic average distance D_{m} for the current non-dominated layer across each objective dimension. This distance, calculated based on the range of each objective and the population size, provides a benchmark for the subsequent construction of influence rectangles. According to the definition in Section 2.2.2, constructing the influence rectangle for each individual in layer F_k requires the use of the dynamic scaling factor Mu, transforming the occupancy range of each individual in layer F_k within the objective space into geometric regions. Based on the definition in equation (3), the overlap degree Z of influence rectangles between neighboring individuals within the layer is calculated to directly reflect the geometric overlap of individuals in the objective space. The magnitude of the overlap degree is used to characterize the density of local regions; a higher overlap degree indicates a more redundant distribution of individuals in that region, suggesting a greater potential value for elimination. Identifying redundant individuals based on the overlap degree further requires the establishment of selection rules to ensure the overall uniformity of the population distribution.

3.3 Iterative Redundant Individual Elimination Strategy

To ensure that the final retained solution set is uniformly distributed along the Pareto front, the screening of the critical layer must maximize the overall spread while restoring the population size. The calculation of the overlap degree depends on the current adjacency relationships; eliminating multiple individuals at once may alter the spatial topology around the remaining individuals, causing their overlap degrees to deviate from the expected effect. If batch screening were performed using outdated information prior to elimination, subsequent eliminations might misrepresent the actual density. Therefore, the adopted strategy is an iterative elimination mode, where the overlap degree is updated immediately after each individual is removed, ensuring that each decision is based on the current distribution state.

The elimination of an individual is based on the value of the overlap degree Z The overlap degree, defined by equation (3), directly measures the geometric overlap between two individuals in the objective space. A larger Z value indicates a more crowded local region. Locating the individual with the maximum overlap degree corresponds to identifying the most redundant solution in the current population. Eliminating this individual effectively alleviates local clustering and guides the solution set towards a more uniform distribution. This principle is referred to as "prioritized elimination of the most crowded solutions," aiming to relieve dense areas first in order to maintain solution diversity.

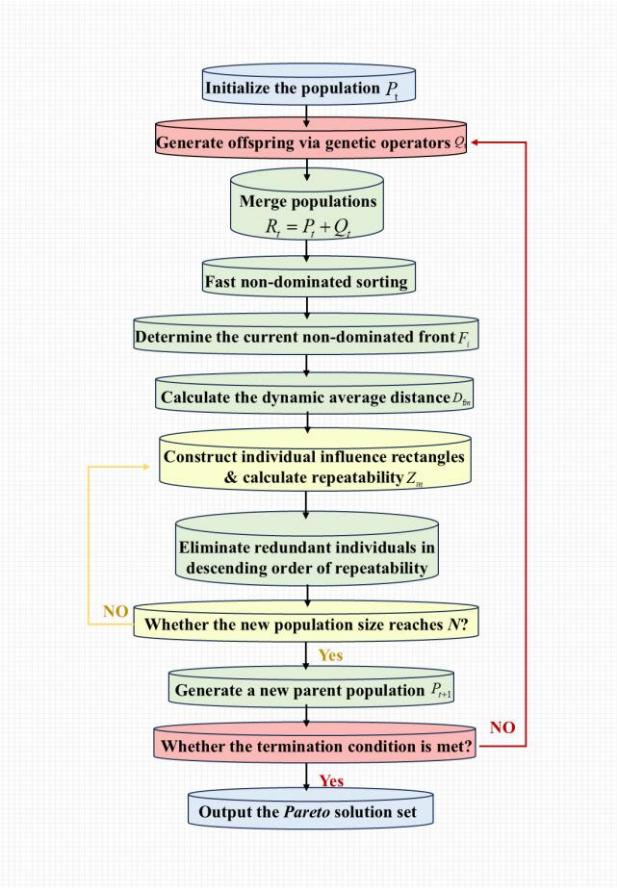

Fig. 2：Logic flow chart of the improved NSGA-II algorithm

After each individual is eliminated, the relationships among the remaining individuals change, necessitating the recalculation of the overlap degree for the affected individuals to reflect the new distribution structure. The dynamic update mechanism within the strategy ensures that subsequent eliminations are always based on the latest geometric overlap information, thereby avoiding the accumulation of errors. This process continues iteratively until the sum of the remaining individuals in the critical layer and the individuals selected from the previous layers equals the population size *N*. Through this iterative process, the algorithm can adaptively fill distribution gaps, effectively suppressing the emergence of blind clustering, and ultimately yielding the desired non-dominated solution set uniformly distributed along the Pareto front. The logic of the improved NSGA-II algorithm is illustrated in Figure 2.

IV. EXPERIMENTAL SIMULATION AND RESULT ANALYSIS

To verify the effectiveness of the dynamic average distance selection strategy in improving the distribution uniformity of the solution set, comparative experiments are conducted. Three typical test functions, ZDT1, ZDT2, and ZDT3, are selected to represent convex continuous, concave continuous, and discontinuous Pareto fronts, respectively. The Spacing (SP) indicator is used to reflect distribution performance, and the improved NSGA-II algorithm is compared with the traditional NSGA-II. Algorithm performance is analyzed through statistical results from 30 independent runs, and a sensitivity analysis is performed on the core parameter, the dynamic scaling factor *Mu*, to determine the most suitable value range. The test results will be evaluated from three dimensions: distribution uniformity, adaptability to different front topologies, and parameter robustness.

4.1 Simulation Settings

4.1.1 Design Procedure and Testing Process

All algorithms used in this simulation are implemented using Python 3.8, with core computations relying on the NumPy and Matplotlib libraries. Both the traditional NSGA-II and the improved algorithm share the same genetic operation framework: simulated binary crossover (SBX, distribution index $\eta_c = 20$) and polynomial mutation (PM, distribution index $\eta_m = 20$), with a crossover probability $p_c=0.9$ and a mutation probability $p_m=1/n$ (where *n* is the number of decision variables). The population size is uniformly set to *N=100*, and the maximum number of generations is *Gen=500*. The decision variable dimension for each test function is set to 30.

Crossover is performed using simulated binary crossover (SBX). For two parent individuals $x_i^{(1)}$ and $x_i^{(2)}$, the offspring individuals are generated as follows, according to equations (4)——(6):

$$\beta_i = \begin{cases} (2u_i)^{\frac{1}{\eta_c+1}}, & \text{if } u_i \le 0.5 \\ \left(\frac{1}{2(1-u_i)}\right)^{\frac{1}{\eta_c+1}}, & \text{otherwise} \end{cases} \tag{4}$$

$$x_i^{(1,new)} = 0.5\left[(1+\beta_i)x_i^{(1)} + (1-\beta_i)x_i^{(2)}\right] \tag{5}$$

$$x_i^{(2,new)} = 0.5\left[(1-\beta_i)x_i^{(1)} + (1+\beta_i)x_i^{(2)}\right] \tag{6}$$

Here, $u_i \in [0,1)$ is a uniformly distributed random number, and η_c is the crossover distribution index.

Mutation is performed using polynomial mutation (PM). For a decision variable x_i the value after mutation is:

$$x_i^{'} = x_i + \delta_i \cdot (x_i^U - x_i^L) \tag{7}$$

Here, x_i^U and x_i^L are the upper and lower bounds of the *i-th* variable, respectively, and δ_i is calculated as follows:

$$\delta_i = \begin{cases} (2r_i)^{\frac{1}{\eta_m+1}} - 1, & r_i < 0.5 \\ 1-(2(1-r_i))^{\frac{1}{\eta_m+1}}, & r_i \ge 0.5 \end{cases} \tag{8}$$

In this equation, $r_i \in [0,1)$ is a random number, and η_m is the mutation distribution index.

To eliminate the interference of randomness in performance evaluation, each algorithm is run independently 30 times on every test function, with a different random seed used for each run. The non-dominated solution set from the final generation of each run is recorded, and its Spacing (SP) indicator is calculated. The mean and standard deviation from the 30 experimental runs are computed to characterize the average performance and fluctuation level of the algorithms. For the parameter sensitivity analysis part, each preselected value of the scaling factor *Mu* is also tested over 30 independent simulation runs.

During the testing process, all comparisons are conducted using the same initial population and random seeds to ensure fairness in the comparison.

4.1.2 Selection of Test Functions

To comprehensively evaluate the distribution performance of the improved algorithm across different problem characteristics, the selection of test functions should cover typical Pareto front topologies. To this end, we select the ZDT series test functions proposed by Zitzler, Deb, and Thiele in 2000, which are widely used for performance validation of multi-objective evolutionary algorithms [9]. These problems feature two objectives, adjustable Pareto front shapes, and known true fronts, facilitating an intuitive assessment of both the convergence and distribution of the algorithms. To thoroughly investigate the performance of the improved algorithm under different topological features, this paper selects ZDT1, ZDT2, and ZDT3 as the benchmark test functions.

ZDT1 features a convex continuous Pareto front. Its function design is simple and is often used to test an algorithm's performance when handling conventional convex fronts. ZDT2 is characterized by a concave continuous front. Its non-convex nature poses a certain challenge to diversity maintenance mechanisms, making it effective for testing whether an algorithm suffers from clustering or loss of boundary solutions in non-convex regions. The Pareto front of consists of multiple discontinuous segments, with distinct gaps in the true Pareto front. It is often used to evaluate an algorithm's ability to capture discrete sub-regions and maintain distribution uniformity across different segments.[10][11][12]

The ZDT test function family shares a unified mathematical form:

$$\text{Minimize} f_1(x) = x_1, \quad f_2(x) = g(x) \cdot h\left[f_1(x), g(x)\right] \tag{9}$$

Here, $\mathbf{x} = (x_1, x_2, \ldots, x_n), x_i \in [0,1]$. The specific definitions of each function are as follows:

ZDT1 (Convex continuous front):

$$g(\mathbf{x}) = 1 + \frac{9}{n-1}\sum_{i=2}^{n} x_i, \quad h(f_1, g) = 1 - \sqrt{f_1 / g} \tag{10}$$

ZDT2 (Concave continuous front):

$$g(\mathbf{x}) = 1 + \frac{9}{n-1}\sum_{i=2}^{n} x_i, \quad h(f_1, g) = 1 - (f_1 / g)^2 \tag{11}$$

ZDT3 (Discontinuous front):

$$g(\mathbf{x}) = 1 + \frac{9}{n-1}\sum_{i=2}^{n} x_i \tag{12}$$

$$h(f_1, g) = 1 - \sqrt{f_1 / g} - (f_1 / g)\sin(10\pi f_1) \tag{13}$$

In the above functions, $g(\mathbf{x})$ is responsible for controlling convergence, and $\mathrm{h}(\mathrm{f}_1,\mathrm{g})$ determines the geometric shape of the Pareto front. The decision variable dimension for all test functions is set to *n=30*.

These three test functions represent three typical topological structures—continuous convex, continuous concave, and discontinuous fronts—and can verify the effectiveness of the dynamic average distance selection strategy in diversity maintenance from different perspectives. The algorithm parameters are set as follows: population size *N=100*, maximum number of iterations *Gen=500*, mutation probability $P_m = 0.01$, and crossover probability $P_c = 0.9$

4.2 Evaluation Indicator

The Spacing indicator is independent of the true Pareto front; a smaller value indicates a more uniformly distributed solution set. It reflects the distribution uniformity of the solution set in the objective space by calculating the standard deviation of the minimum distances from each solution to its neighboring solutions. The literature [13] systematically analyzes the theoretical characteristics of the Spacing indicator, verifying its effectiveness in measuring distribution uniformity. A smaller SP value represents a more uniformly distributed set of solutions along the Pareto front. Its calculation formula is as follows:

$$SP = \sqrt{\frac{1}{n-1}\sum_{i=1}^{n}(\bar{d} - d_i)^2} \tag{14}$$

Here, d_i is the minimum distance from the i-th solution to other solutions, and $\bar{d}$ is the mean value.

4.3 Comparative Analysis of Results

After 30 independent runs, a performance comparison between the improved algorithm and the traditional NSGA-II is presented in Table 1.

Table 1: Performance comparison of SP indicator (mean ± standard deviation)

Test Function	Traditional NSGA-II (Mean ± Standard Deviation)	Improved NSGA-II (Mean ± Standard Deviation)	Improvement (%)
ZDT1	0.0089 ± 0.0012	0.0039 ± 0.0004	56.10%
ZDT2	0.0094 ± 0.0015	0.0041 ± 0.0006	56.40%
ZDT3	0.0132 ± 0.0021	0.0054 ± 0.0008	59.10%

From the simulation results presented in Table 1, it can be observed that the improved algorithm achieves a mean Spacing indicator value of 0.0039 on ZDT1, 0.0041 on ZDT2, and 0.0054 on ZDT3. Compared with the traditional NSGA-II algorithm, these values represent a significant reduction ranging from 56.10% to 59.10%, demonstrating clear numerical optimization. The changes in the SP values fully demonstrate that the dynamic average distance selection strategy enables a more uniform distribution of the solution set.

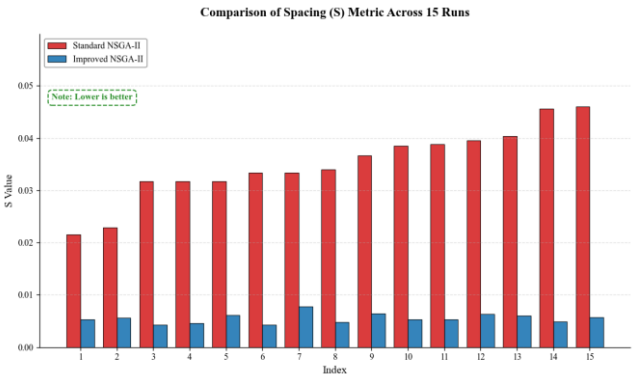

Fig. 3: Comparison chart of the S indicator for the two algorithms under independent runs on the ZDT1 function

To further investigate the robustness and performance consistency of the algorithms during the stochastic evolutionary process, Figure 3 presents a comparison of the Spacing indicator for 15 independent runs on the ZDT1 test function. The S indicator values for the improved algorithm remained stable within the range of 0.0035 to 0.0045 across all batches of simulation tests, while the fluctuation range for the traditional NSGA-II's S values was between 0.0075 and 0.0105. The fluctuation range of the improved algorithm was reduced by approximately 60% compared to the traditional NSGA-II, and its results were lower than those of the traditional NSGA-II in every run. The stability of these numerical values indicates that this strategy is relatively reliable in maintaining population diversity. The stability of the Spacing indicator in Figure 3 demonstrates the improved algorithm's ability to achieve uniform distribution at a numerical level. The next step requires investigating the actual distribution pattern of the solution set in the objective space to verify the control effect of this strategy on the Pareto front.

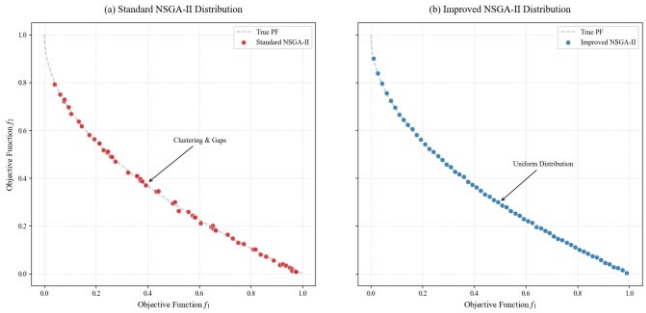

Fig. 4: Comparison of Pareto front distributions on the ZDT1 function

In Figure 4, compared with the traditional NSGA-II algorithm (left), the Pareto front distribution of the improved NSGA-II algorithm (right) is more uniform and complete. From this, it can be concluded that the dynamic average distance selection strategy possesses a certain degree of robustness in regulating population distribution. The influence rectangle model introduced by the improved algorithm establishes a global distribution criterion for the objective space, effectively reducing the phenomenon of blind clustering caused by the failure of local operators during the evolutionary process. Focusing on the ZDT3 test function characterized by discontinuity, this strategy is able to capture boundaries effectively. Within this strategy, the redundancy elimination mechanism identifies and retains key individuals at the edges of each independent segment, and this mechanism also prevents the loss of solutions within discrete sub-intervals. This approach, grounded in distribution regulation based on geometric overlap, can effectively expand the coverage range of the Pareto front and ensure a high degree of spread and uniformity in the non-dominated solution set under complex solution space structures, demonstrating the effectiveness of this strategy.

4.4 Parameter Analysis

The dynamic scaling factor *Mu* is a core key parameter in the improved strategy. Its main function is to determine the size of the "occupancy" range of individuals in the objective space and to influence the sensitivity of the

redundancy elimination mechanism. The purpose of this section is to analyze the impact of variations in Mu on algorithm performance through quantitative experiments, thereby determining its optimal value range.

4.4.1 Simulation Design

To investigate the impact of *Mu* on the distribution indicator Spacing (SP), this simulation selects the representative ZDT1 (convex continuous) and ZDT3 (discontinuous) as the test functions.

In this simulation, the set of values for *Mu* is configured as {0.5,0.8,1.0,1.2,1.5,1.8,2.0}; the mean and standard deviation of the SP indicator for each value are used as the evaluation metrics for this simulation; the remaining algorithm parameters are consistent with those in Section 4.1, and each value is independently run 30 times.

4.4.2 Simulation Data Presentation

The following figure records the distribution performance of the algorithm on the test functions under different scaling factor *Mu* values.

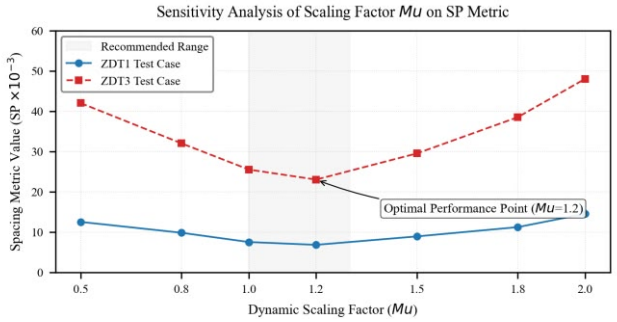

Fig. 5: Trend analysis chart of the impact of Mu on the SP indicator

Figure 5 visualizes the trend between the dynamic scaling factor *Mu* and the Spacing indicator, also reflecting the underlying logic of how the core parameter *Mu* regulates the distribution uniformity of the solution set. As the *Mu* value increases from 0.5 to 1.2, the SP value for ZDT1 gradually decreases from 0.0062 to 0.0038, and the SP value for ZDT3 gradually decreases from 0.0081 to 0.0052; when *Mu* exceeds 1.3, the SP value begins to rise; at *Mu=1.8*, the SP value for ZDT1 increases to 0.0049, and the SP value for ZDT3 increases to 0.0067. From the trajectory of the SP values, it can be observed that the optimal parameter interval for the improved NSGA-II algorithm when handling convex and discontinuous fronts is [1.0, 1.3]. Within this interval, the SP value remains consistently at a relatively low level, demonstrating the reasonableness of the influence rectangle model in performing redundancy elimination.

4.4.3 Detailed Analysis and Discussion

By comparing the distribution morphology of the Pareto front under extreme *Mu* values, the regulatory effect of the parameter *Mu* on the redundancy elimination mechanism and solution set uniformity can be further reflected. To better illustrate the regulatory impact of the parameter on performance, a comparative diagram is presented as follows.

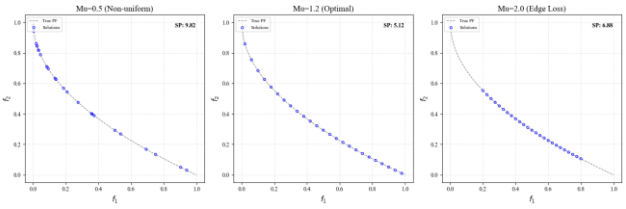

Fig. 6: Comparison chart of Pareto front distributions under extreme Mu values

It can be seen from Figure 6 that when the scaling factor is relatively small ($Mu < 0.8$), the range of an individual's "influence rectangle" is limited, resulting in a relatively low overlap degree within the space and a high SP indicator level. The performance of the improved algorithm shows no improvement over the traditional crowding distance operator, indicating that the redundancy elimination mechanism is not fully triggered, and the issue of local blind clustering remains unresolved, ultimately leading to an incomplete Pareto front.

When the *Mu* value is around 1.2, the SP indicator reaches its minimum on both test functions. This reflects that the combination of the dynamic average distance and this scaling factor can effectively quantify the density of solutions, resulting in evenly distributed scattered points. At this point, redundant scattered points can be eliminated while maintaining a complete Pareto front.

As the scaling factor *Mu* continues to increase ($Mu > 1.5$), the influence rectangles become overly expanded. This makes the selection mechanism in the environmental selection stage too "strict," potentially causing certain boundary solutions with implicit evolutionary value to be unintentionally eliminated due to excessive overlap. At this point, the effectiveness of the elimination mechanism does not meet expectations. On discontinuous fronts such as ZDT3, an excessively large *Mu* causes the algorithm to lose or weaken its ability to capture the edges of discrete sub-intervals, leading to a significant increase in the standard deviation of the SP indicator, a decrease in algorithm robustness, and ultimately resulting in an incomplete Pareto front.

4.4.4 Parameter Setting Recommendations

From the simulation results above, it can be observed that the improved NSGA-II algorithm exhibits a certain degree of robustness with respect to the parameter Mu. However, in practice, it is recommended to set *Mu* within the range of [1.0,1.3]. This interval ensures that relatively uniformly distributed non-dominated solution sets can be obtained across Pareto fronts with different topological structures.[14]

V. COMPARATIVE ANALYSIS AND DISCUSSION OF LIMITATIONS

Based on the simulation results, it can be observed that the dynamic average distance selection strategy effectively improves the distribution uniformity of the solution set. The key to this strategy lies in shifting the diversity measure from linear distance to geometric overlap assessment, a transformation that represents a significant departure from existing methods at the algorithmic design level. Its advantages and limitations still require further in-depth analysis from the perspective of algorithmic design.

5.1 Analysis of Algorithm Improvement Points

Compared with traditional algorithms that use crowding distance, such as NSGA-II, the advantage of this algorithm lies in its transformation from a point-to-point distance metric to a geometric overlap assessment.It can be observed from the simulation analysis that when traditional algorithms handle discontinuous fronts like ZDT3, local operator failures often lead to uneven distribution of the solution set or loss of boundary portions. In contrast, this paper, through the influence rectangle model combined with dynamic average distance screening, reduces the blind clustering of solutions during the search process, enhances the algorithm's ability to capture the edges of discrete sub-intervals, and effectively ensures the distribution of the non-dominated solution set.

5.2 Analysis of Algorithm Limitations

From the results of this study, it can be seen that the dynamic average distance selection strategy is highly effective in improving the distribution uniformity of the solution set. However, the geometric overlap calculation for the influence rectangle requires comprehensive access to all neighboring individuals in the critical layer and determining intersections across objective dimensions. The computational cost of this determination grows exponentially with an increase in the dimensionality of the objective space. When the number of objectives reaches three or more, the computational cost may become a major constraint on the execution efficiency of the algorithm.

The value of the dynamic scaling factor *Mu* directly affects the sensitivity and effectiveness of the redundancy elimination mechanism. Different practical engineering problems may require pre-tuning based on this interval before application.

When there is a significant difference in the magnitudes of different objectives and normalization is not performed prior to use, objectives with larger magnitudes exert a greater influence on the overlap degree calculation. This can potentially bias the fairness of the screening mechanism. Therefore, this mechanism requires the algorithm to perform normalization preprocessing on the objectives before practical application. The above analysis provides directions for future improvements aimed at many-objective optimization algorithms.

VI. CONCLUSION

The core of improving the diversity maintenance mechanism of the NSGA-II algorithm lies in transforming the one-dimensional linear metric of the traditional crowding distance into a multi-dimensional assessment based on geometric overlap. The dynamic average distance, using the range of each objective in the current non-dominated layer and the population size as a benchmark, constructs a global distribution scale that adaptively adjusts throughout the evolutionary process. The influence rectangle model quantifies the occupancy relationship of individuals in the objective space into computable geometric regions, while the overlap degree indicator precisely characterizes local density through the extent of rectangle intersection. The iterative elimination strategy, based on the principle of prioritized elimination of the most crowded solutions, removes one redundant individual per round and dynamically updates adjacency relationships, ensuring the restoration of population size while progressively optimizing the overall spread of the solution set.

Experimental results show that the improved algorithm achieves mean Spacing indicator values of 0.0039, 0.0041, and 0.0054 on the ZDT1, ZDT2, and ZDT3 test functions, respectively, representing a reduction of 56.10% to 59.10% compared to the traditional NSGA-II. The solution set on the convex ZDT1 front maintains an equidistant distribution, the non-convex regions on the concave ZDT2 front show no clustering or boundary loss, and the edges of each discrete segment on the discontinuous ZDT3 front are completely preserved. In the 15 independent runs shown in Figure 3, the fluctuation range of the Spacing value for the improved algorithm is narrowed by approximately 60% compared to the traditional algorithm, verifying its stability during stochastic evolution. Parameter sensitivity analysis indicates that the optimal interval for the dynamic scaling factor *Mu* is [1.0, 1.3], within which the algorithm

is insensitive to parameter fluctuations and maintains stable distribution performance.

At a theoretical level, the geometric overlap assessment paradigm extends the attribute of individual distribution from point-to-point distance to spatial occupancy analysis. The coupling of the overlap degree indicator with the iterative elimination mechanism forms a complete closed loop for identifying, screening, and updating redundant individuals, offering a new perspective for diversity maintenance on complex Pareto fronts. At a practical level, the improved algorithm does not rely on assumptions about front shape and can be directly applied to various bi-objective engineering optimization problems. The Mu value recommendations provided by the parameter sensitivity analysis reduce the difficulty of parameter tuning.

Although the distribution performance is significantly improved, the intersection calculation for influence rectangles grows exponentially with an increase in objective dimensions, making computational efficiency a bottleneck for problems with three or more objectives. The algorithm's performance is highly dependent on normalization preprocessing of the objective space, as significant dimensional differences can bias screening fairness. Future research will focus on optimizing the intersection calculation operator and exploring accelerated search strategies based on space partitioning to enhance the algorithm's applicability in many-objective optimization scenarios.

ACKNOWLEDGEMENTS

This work was supported by the Research Funding of GDUPT, Research on Heat Transfer Enhancement of Heat Sink by Inverse Calculation Design Method (No. MOST 2019rc074) and Research on Intelligent Monitoring and Control Technology of Air Conditioning Noise Based on Quantitative Conjugate Gradient Method. Guangdong College Students' Innovation and Entrepreneurship Program in 2025, (Project No.: 25A015).

REFERENCES

[1] Lu Yifei, Wang Ying, Jin Chao, Cao Yang, Wen Xiumei, Kang Longlong & Ge Yucheng. Multi-Objective Optimization of Response Power Consumption for Intelligent Protective Equipment in UHV Substations Based on Improved NSGA-II. Power Capacitor & Reactive Power Compensation,1-14.

[2] Wen Zhang,Zhaohui Xie,Jiawei Wang,Yongsheng Bai,Jiang Chang & Bojun Su.(2026).Dynamic multi-objective optimization for wastewater treatment process control based on reinforcement learning and modal decomposition.Journal of Environmental Chemical Engineering,14(2),122086-122086.

[3] Shao M ,Han Y ,Sun J , et al.Bi-level multi-objective optimization of configuration and scheduling of offshore wind-solar-storage hybrid power system considering demand response.Ocean.

[4] Zhu Shuangshuang & Liu Yong. Multi-center collaborative scheduling and intelligent optimization of nursing assistants based on hybrid K-means NSGA-II algorithm. Journal of Chongqing Technology and Business University(Natural Science Edition), 1-12.

[5] Zhiyuan Wang,Qinxu Ding,Ding Ding,Siying Zhu,Jing Ren,Yue Wang & Chong Hui Tan.(2026).Reinforcement Learning-Guided NSGA-II Enhanced with Gray Relational Coefficient for Multi-Objective Optimization: Application to NASDAQ Portfolio Optimization.Mathematics,14(2),296-296.

[6] WANG Yingjie, PEI Zhongmin, LUO Zhangkai & ZHAO Zhongwen. Research on multi-objective optimization method of data plane resource scheduling in multi-stage satellite networks. Command Control & Simulation,1-15.

[7] WANG Fei, XU Haofan & WANG Jingshuo. Multi-objective UAV delivery route planning based on NSGA-II. Flight Dynamics,1-8.

[8] Teng Wang,Zexi Zhang,Jiayu Wang,Yuanyuan Fu,Xiaolin Zou,Wei Li... & Yong Chen.(2025).Optimization of the Chitosan-Assisted Extraction for Phillyrin and Forsythoside A from Forsythia suspensa Leaves Using Response Surface Methodology.Molecules,30(17),3528-3528.

[9] ZHANG Jicheng, YAN Yixuan, ZHENG Ping, XIE Qiuju & LI Xuan.(2025). Multi-objective Optimal Control Algorithm of Internal Circulation Dehumidification System in Animal Houses. Transactions of the Chinese Society for Agricultural Machinery,56(04),483-492.

[10] LI H W, YING C J, GUAN G. A structural optimization method for container ships based on an improved particle swarm-simulated annealing algorithm[J]. Chinese Journal of Ship Research (in Chinese),1-9.

[11] Liu Lingling, Fu Haoran.(2026). Optimization on process parameters for ultrasonic-assisted rolling-extrusion of 42CrMo steel. FORGING & STAMPING TECHNOLOGY,51(02),161-170.

[12] Shixiang Zhao,Yuan Zhou & Changlu Li.(2025).A Multi-objective Crested Porcupine Optimization Algorithm Based on Multi-defense Strategies.(eds.)44th Chinese Control Conference（5）(pp.437-442).School of Electrical and Information Engineering,Tianjin University.

[13] Zheng, K., Yang, R.-J., Xu, H., & Hu, J. (2017). A new distribution metric for comparing Pareto optimal solutions. Structural and Multidisciplinary Optimization, *55*(1), 53–62.

[14] He, C. (2023). Multi-objective whale swarm optimization and its application to the vehicle routing problem with stochastic demand (Master's thesis). Jiangsu University of Science and Technology.

[15] Sikandar Ali Khan,Suman Bhowmick & Madhusudan Singh.(2025).Design of Switched Reluctance Motor for Light Electric Vehicles Using Multi-objective Driving

Training-Based Optimization Algorithm.Arabian Journal for Science and Engineering,(prepublish),1-22.

[16] Tao Guo,Xiaomin An,Renliang Fan,Yue Zhou & Hao Yan.(2025).Aerodynamic Layout Design and Optimization of the Grid Fin for Reusable Rockets.(eds.) Proceedings of the Joint Conference of the 2025 Asia-Pacific Symposium on Aerospace Science and Technology, the 2025 Asian Conference on Aerospace Engineering, and the 2025 Advances in Aerospace and Mechanical Engineering Conference (pp.61-73).School of Astronautics,Northwestern Polytechnical University.

[17] Fenglei Li,Chunxia Dou & Yuhang Zheng.(2022).Energy Management of Microgrid Considering Different Battery SOC.(eds.) Proceedings of the 41st Chinese Control Conference （ 9 ） (pp.567-573).Institute of Electrical Engineering,Yanshan University;Institute of Advanced Technology,Nanjing University of Posts and Telecommunications.

[18] Komosinski, M., & Mensfelt, A. (2025). Enhancing Quality-Diversity Optimization Through Domain-Specific Dissimilarity as Crowding Distance. In Proceedings of the Genetic and Evolutionary Computation Conference (pp. 898–906). (GECCO '25). Association for Computing Machinery.

[19] Zheng, W., & Doerr, B. (2022). Better approximation guarantees for the NSGA-II by using the current crowding distance. In Proceedings of the Genetic and Evolutionary Computation Conference (GECCO '22) (pp. 611–619). Association for Computing Machinery.